Graphene Hot Paper

How to cite: *Angew. Chem. Int. Ed.* **2022,** *61*, e202200321
International Edition: doi.org/10.1002/anie.202200321
German Edition: doi.org/10.1002/ange.202200321

Demonstrating and Unraveling a Controlled Nanometer-Scale Expansion of the Vacancy Defects in Graphene by CO_2

*Mojtaba Rezaei, Luis Francisco Villalobos, Kuang-Jung Hsu, and Kumar Varoon Agrawal**

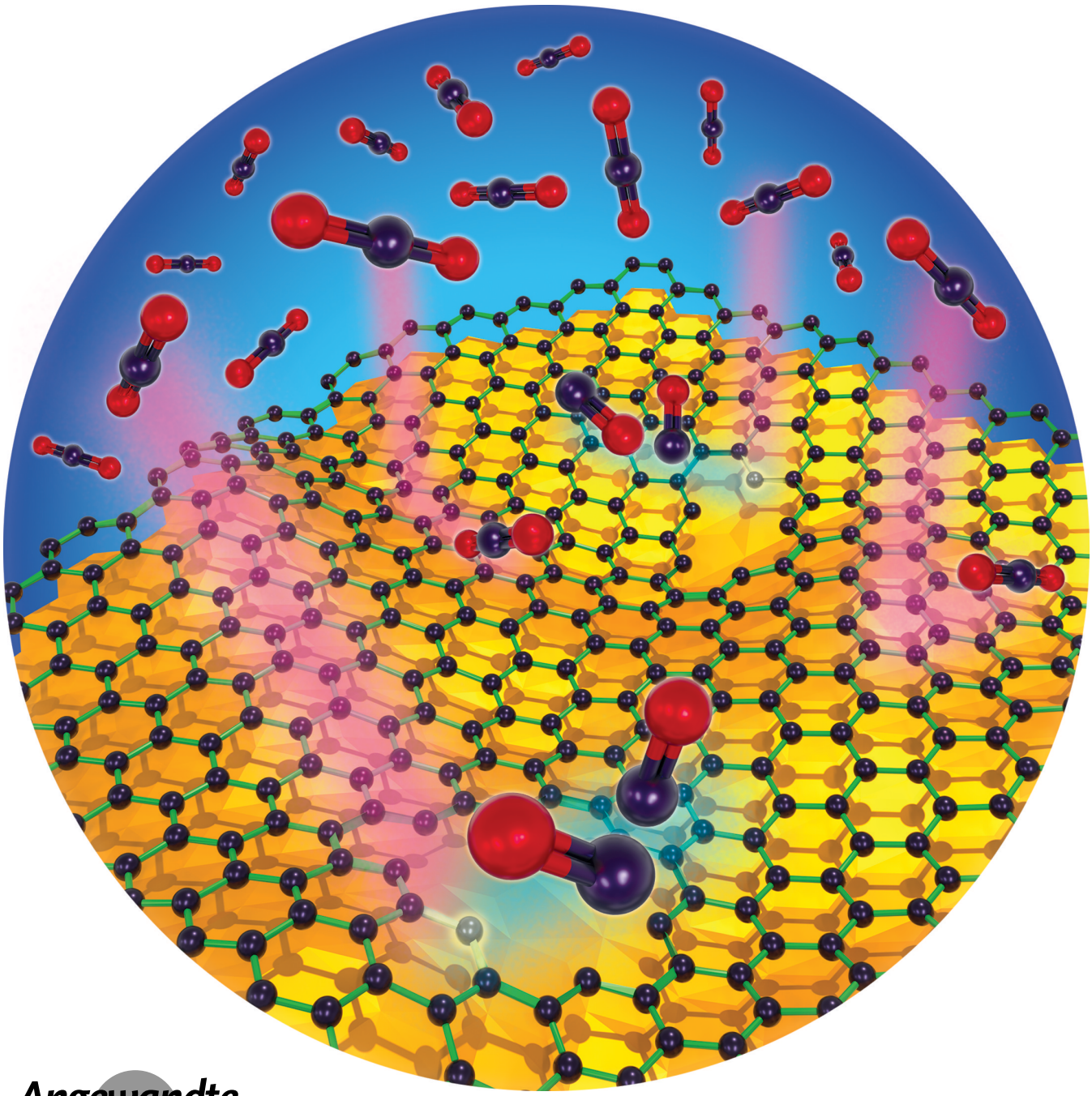

Abstract: A controlled manipulation of graphene edges and vacancies is desired for molecular separation, sensing and electronics applications. Unfortunately, available etching methods always lead to vacancy nucleation making it challenging to control etching. Herein, we report CO_2-led controlled etching down to 2–3 Å per minute while completely avoiding vacancy nucleation. This makes CO_2 a unique etchant for decoupling pore nucleation and expansion. We show that CO_2 expands the steric-hindrance-free edges with an activation energy of 2.71 eV, corresponding to the energy barrier for the dissociative chemisorption of CO_2. We demonstrate the presence of an additional configurational energy barrier for nanometer-sized vacancies resulting in a significantly slower rate of expansion. Finally, CO_2 etching is applied to map the location of the intrinsic vacancies in the polycrystalline graphene film where we show that the intrinsic vacancy defects manifest mainly as grain boundary defects where intragrain defects from oxidative etching constitute a minor population.

Introduction

Defect generation in graphene by oxidation has been widely studied due to the inherent uniformity and scalability of the oxidation-based defect generation.[1] Most of the early studies focused on the interaction of graphite with strongly oxidizing agents such as those related to Hummer's method or with gaseous O_2 at high temperature.[2–4] However, under these harsh environments, the oxidation reaction is difficult to control especially when the goal is to control the size of vacancy defects at the nanometer and sub-nanometer length scales or to precisely shape the graphene edges. Availability of an oxidation method that controllably etches the graphene lattice at the rate of a few atoms per seconds can tune the size of vacancy defects in graphene for molecular separation and sensing. Such methods can also be applied for precisely shaping the width of graphene nanoribbons for band-gap optimization[5,6] with application in electronics and optoelectronics. This would also allow shaping graphene nanomeshes,[7] quantum dots,[8] and nano disks[6] with a high degree of control. Especially in the field of separations, such a technique can be used to tune the pore size for several molecular and ionic-sieving applications, e.g., organic solvent nanofiltration,[9] ion-ion separation,[10] dialysis,[11] etc.

As of now, there is no method to etch graphene edge without nucleating a new vacancy defect in the basal plane of graphene. For example, treatment of graphene with O_2[12] and O_3[13,14] results in generation of new vacancy defects. In this context, CO_2 is a promising mild etchant where the energy barrier for the nucleation of single vacancy defect is predicted to be prohibitively large (5.0 eV).[15] In principle, carbon gasification by CO_2 is the Boudouard reaction ($C + CO_2 \leftrightarrow 2\,CO$).[16] Ab-initio calculations have reported energy barrier for the gasification of graphene edge by CO_2 in the range of 2.5–4.6 eV. For example, Zhang et al. reported activation energies for the dissociative chemisorption of CO_2 on a single vacancy defect, 55–77 defect, and 555–777 defect as 2.50, 2.80, and 3.30 eV, respectively.[17] The activation energies for the dissociative chemisorption of CO_2 on zigzag and armchair edges have been estimated to be 2,6 and 4.6 eV, respectively.[18]

The literature probing the mechanism of interaction of CO_2 with defects in graphene suggest the following reaction pathway: i) physisorption of CO_2 on top of the defective site, ii) chemisorption of CO_2 on the defective site resulting in the formation of a lactone and/or semiquinone group, and iii) evolution of the terminal groups followed by the desorption of two CO molecules.[19–22] However, the nature of the CO_2 chemisorption sites (single vacancy, double vacancy, armchair and zigzag edge, etc.), the identity of the intermediate species formed by chemisorption (lactone vs. semiquinone), and the underlying assumptions of the computational methods have resulted in a large discrepancy in the computed energy barrier for the rate-limiting step (1.7–4.6 eV)[18,22–24] and there is no clear consensus on the energy barrier.

Experimental studies on probing reaction of CO_2 with graphene edges or vacancies are extremely rare. In fact, currently, there are no systematic studies probing the reaction kinetics of CO_2 with defects in graphene. Recently, Yang et al.[25] reported dependence of the etching rate on the etching temperature and CO_2 flow rate, and demonstrated that CO_2 does not nucleate new defects in the graphene basal plane up to 1000 °C. However, etching kinetics was not reported because the reaction was not controlled effectively leading to a large heterogeneity in the resulting features, e.g., fully-etched graphene in certain area, graphene with etched trenches in some area, and faceted pores in other areas.

Herein, for the first time, we report controlled and uniform etching of graphene with CO_2 in the temperature range of 750–1000 °C and extract the energy barrier for the expansion of large edges in graphene as 2.7 eV, corresponding to the chemisorption energy barrier of CO_2 on zigzag edges in graphene. We establish an etching regime that is not limited by the CO_2 mass transfer from the bulk to the graphene edges and study the vacancy expansion rate by adjusting etching temperature and time. We show that nanometer-scale vacancies can be expanded at an attractive rate of 2–3 Å min^{-1} making this route highly promising for tuning the pore size in graphene for molecular separation

[*] M. Rezaei, L. F. Villalobos, K.-J. Hsu, K. V. Agrawal
Laboratory of Advanced Separations (LAS)
École Polytechnique Fédérale de Lausanne (EPFL)
1950 Sion (Switzerland)
E-mail: kumar.agrawal@epfl.ch

and sensing application. We show the presence of an additional configurational energy barrier for CO_2 to chemisorb at the edge of nanometer-sized vacancies resulting in an order of magnitude slower rate for the smaller vacancies, with no expansion for defects smaller than 0.15 nm. We demonstrate that CO_2 does not nucleate new vacancy defects resulting in a gaussian pore-size-distribution (PSD) of the expanded pores, in sharp contrast to the lognormal PSD typically achieved using oxidative etching methods. Finally, CO_2 etching allows one to map the locations of intrinsic vacancy defects in graphene by transmission electron microscopy, which has been proven a challenging task attributing to their low density. This allows us to establish two distinct origins of the intrinsic vacancy defects: i) incomplete intergrowth of misaligned graphene grains, and ii) etching of the lattice in the presence of residual O_2 in the reactor. Our findings demonstrates that CO_2 can be used for structuring graphene films down to the length-scale of a nanometer for various applications such as molecular separation and sensing.

Results and Discussion

Single-layer graphene was synthesized on a Cu foil by the chemical vapor deposition (CVD) approach using CH_4 as the carbon precursor (schematic in Figure S1).[26] The synthesized graphene was high-quality with a low density of intrinsic defects as indicated by the mapping data based on Raman spectroscopy[27] (I_{2D}/I_G of 1.51 ± 0.25; I_D/I_G of 0.04 ± 0.02, Figure S2). The intrinsic defects are composed of vacancy defects which have been argued to form at the grain boundary or to result from a limited oxidation of the lattice in the residual O_2 in the reactor.[28–31] Based on the carbon amorphization trajectory[27] and gas permeation studies,[32] the density of intrinsic vacancy defects corresponds to $\approx 10^{10}\,cm^{-2}$. These defects are the starting point for this study. Unless otherwise specified, CO_2 etching was carried out immediately after the graphene synthesis inside the CVD reactor, allowing us to conduct etching studies on contamination-free graphene surface with a CO_2 partial pressure of 500 mTorr, a condition where CO_2 mass transfer from bulk to graphene edges is not rate limiting (see discussion later).

Scanning electron microscopy (SEM) of vacancies expanded at 1000 °C for 1.5 min revealed large, faceted defects (Figure 1b, Note S1), independent of Cu grain orientation (Note S2) with defect density of $1.2\times10^8\,cm^{-2}$ with a gaussian size distribution (0.45 ± 0.07 μm, Figure 1c, also see characterization procedure 2.7 in Supporting Information) as against lognormal distribution that is typically observed when nucleation and pore expansion are concomitant.[9,33,34] The small bright dots visible in Figure 1b and d are SiO_x particles deposited during the annealing process due to the reaction of Cu vapor with the quartz reactor during its reversible phase transition from α-quartz to β-quartz at 573 °C.[35] A higher resolution SEM image and the corresponding EDX spectra of these particles confirm their identity (Figure S3). They can be eliminated by isolating quartz from Cu, e.g., by placing a high purity alumina tube inside the quart reactor.[36]

We assign the faceted defects as the expanded intrinsic vacancy defects for the reasons described below. The features are brighter than the surrounding graphene because of the higher yield of secondary electrons from bare Cu (CVD substrate) compared to graphene-covered Cu. When we oxidized the sample in ambient air at 160 °C for 60 min, a method that has been used in the past to visualize CVD graphene as well as defects in CVD graphene,[37,38] the faceted features were severely oxidized whereas the rest of the sample was unaffected (Figure 1d). We prepared another sample by CO_2 etching (900 °C for 150 min) and transferred the graphene from Cu foil to SiO_2/Si wafer. Optical microscopy of the resulting sample revealed the etched features had a contrast that was similar to that of the bare wafer further indicating that the features were expanded vacancy defects (Figure 1e, S4). Raman spectroscopy of one of these features also conclusively confirmed this as the intensity of the *G* and *2D* peaks dropped to zero inside the faceted features while typical spectra characterizing high-quality single-layer graphene could be readily obtained from the area surrounding the holes (Figure 1f).[39] A mapping of the 2D peak intensity also clearly proves this point. The 2D peak intensity remains uniform for the graphene-covered area, and it drops to zero for the expanded vacancy defect (Figure 1g and S4). The mapping of the surrounding area yielded I_D/I_G ratio of 0.04 ± 0.02 confirming that graphene domains surrounding the expanded vacancy defect is not affected by the high-temperature CO_2 treatment. This indicates that the etching takes place only at an existing defect site (see further discussion on this later). We note that CO_2 does not oxidize the Cu surface even at 1000 °C making CO_2 an excellent etchant for CVD graphene (Figure S16, Note S3).

The size of the expanded defect had a straightforward correlation with the etching time indicating that the etching reaction was not limited by the mass transfer of CO_2 from the bulk to the graphene edge (Figure 2a). For example, etching times of 15 and 60 min yielded smaller pores with size distributions of 0.44 ± 0.06 and 1.80 ± 0.12 μm, respectively, compared to that of 4.87 ± 0.32 μm at 150 min at 900 °C (Figure 2a and S5). Again, the size distributions had a gaussian profile at all etching times. A fitting between the pore size and etching time resulted in a straight line passing through the origin corresponding to an etching rate of $31.40\pm1.05\,nm\,min^{-1}$ (Figure 2b). The density and average center to center distance between the pores did not change when the etching time was increased from 15 to 150 min confirming that the nucleation of vacancy defects did not occur with CO_2 (Figure 2c,d).

We could controllably expand the intrinsic vacancies using CO_2 with expansion rate increasing from 0.60 to $280\,nm\,min^{-1}$ by increasing the etching temperature from 750 to 1000 °C (Figure 3a, S6). In fact, the pore expansion rate had an exponential dependence on the CO_2 exposure temperature. An Arrhenius-type dependence of expansion rate on the etching temperature could be fitted with a high goodness of fit ($R^2=0.994$) yielding an activation energy of

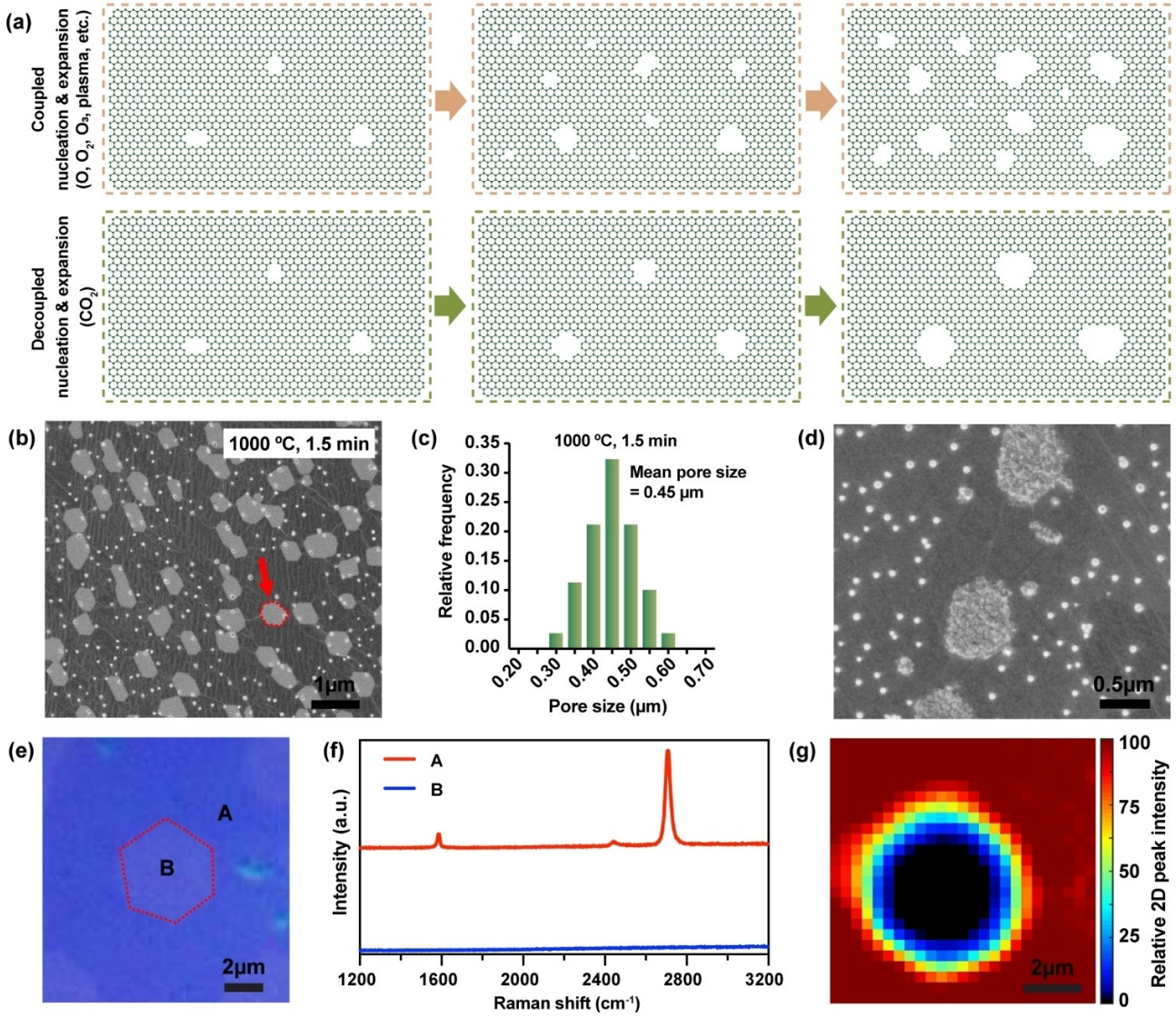

Figure 1. a) Schematic representation of etching of graphene with CO_2 and traditional oxidants (e.g., O_2, O_3, O_3/UV, etc.). While CO_2 does not nucleate new defects and only expands existing vacancies, the other oxidants result in new nucleation events. b) SEM image of expanded vacancy defects (lighter areas) in graphene (darker areas) by 500 mTorr CO_2 on Cu foil at 1000 °C for 1.5 min (a typical expanded pore is highlighted with red dashed lines and an arrow), and c) the corresponding size distribution. d) SEM image of the sample shown in panel b after annealing in air at 160 °C for 60 min, revealing the oxidized Cu domains at the site of vacancy defects. e) Optical image of a vacancy defect expanded at 900 °C for 150 min after being transferred onto a SiO_2/Si substrate. Lighter area is the expanded vacancy defect, and the darker area is the remaining graphene. The expanded pore is highlighted with red dashed lines. f) Raman spectra of points A and B marked on the optical image shown in panel e. g) The corresponding Raman spectroscopy mapping of the area marked by the red rectangle in panel e.

262 kJ mol^{-1} or 2.7 eV (Figure 3b). As per the theoretical predictions, CO_2 binding at a defect site in graphene proceeds with a dissociate adsorption which is also the rate-limiting step. For instance, the energy barrier of etching of graphene zigzag and armchair edges have been reported to be 2.6 and 4.6 eV, respectively,[18,40] where the lower barrier for zigzag edge is reasonable given the lower stability of zigzag edges compared to armchair edges.[41] Based on this, we attribute this observed activation energy (2.7 eV) as the energy barrier for the dissociate chemisorption of CO_2 on the zigzag edge of graphene (Figure S7).

We note that the energy barrier for the dissociate chemisorption of CO_2 is expected to be function of the initial defect size where steric hindrance for fitting the CO_2 to the defect site plays an important role especially for nanometer-scale vacancy defects where CO_2 cannot fit inside the defect. Therefore, the estimated energy barrier (2.7 eV) corresponds only for the expansion of larger vacancies (>2 nm in size, also see discussion later) which do not present steric hinderance for CO_2 chemisorption. This is proven by the fact that we observed an exponential dependence of the density of expanded vacancy defects on the etching temperature (2.5×10^5, 1.7×10^6, 4.3×10^6, 3.0×10^7,

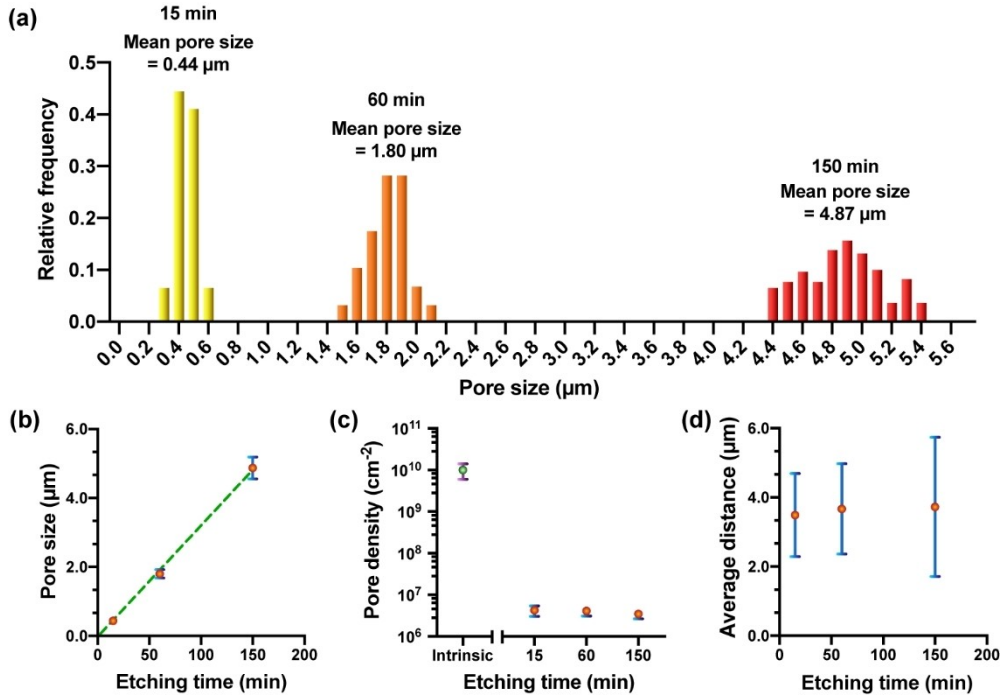

Figure 2. a) The histogram of PSD of the expanded vacancy defects in samples etched by CO_2 at 900 °C for 15, 60, and 150 min. b) Expanded pore size versus etching time for the samples shown in panel a, displaying the linear etching behavior of CO_2 regarding etching time. c) Density of expanded pores as a function of etching time compared to that of intrinsic vacancy defect and d) average distance between the expanded pores as a function of etching time. The error bars in all panels refer to standard deviation. For panel (b), they refer to pore size based on analysis of over 300 pores. For panels (c) and (d), they refer to pore density for analysis of over 20 different areas.

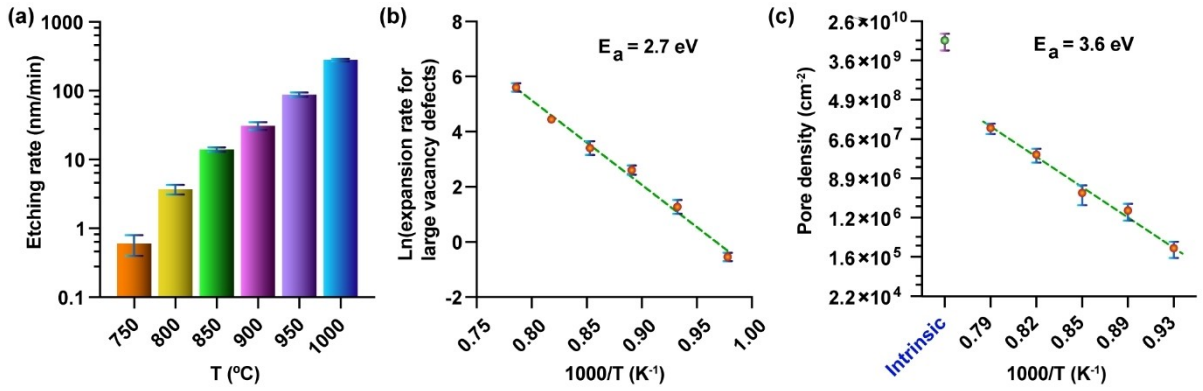

Figure 3. a) Etching rate of graphene as a function of temperature (750–1000 °C). Arrhenius plot for the expansion rate of large vacancies (b). Linear behavior of the natural logarithm of the etching rate versus the reciprocal of the etching temperature at 500 mTorr CO_2. c) Density of expanded pores (natural logarithm scale) versus the reciprocal of the etching temperature at 500 mTorr CO_2. The error bars in all panels refer to standard deviation. For panel (a) and (b), they refer to etching rate based on analysis of over 300 pores. For panel (c), they refer to pore density for analysis of over 20 different areas.

and $1.2\times10^{8}\,cm^{-2}$ at 800, 850, 900, 950, and 1000 °C, respectively) corresponding to an activation energy of 343 kJ mol^{-1} or 3.6 eV (Figure 3c). The density of expanded defects, even for the case of the highest temperature (1000 °C), remains more than two orders of magnitude lower than the density of intrinsic vacancy defects ($\approx10^{10}\,cm^{-2}$) in the as-synthesized graphene. We note that this does not imply nucleation of a new vacancy defect on basal plane of graphene at higher temperatures. It implies that expansion of the smaller defects with steric hinderance for CO_2 chemisorption is activated at higher temperature.

The presence of higher energy barrier for nanometer-scale vacancies manifested in a slower expansion of these defects. We used high-resolution transmission electron microscopy (HRTEM) and scanning transmission microscopy (STM) in combination with SEM to probe small defects. For larger defects, we observed an expansion rate of ≈3.5 nm min^{-1}, independent of the size of the defect (160–

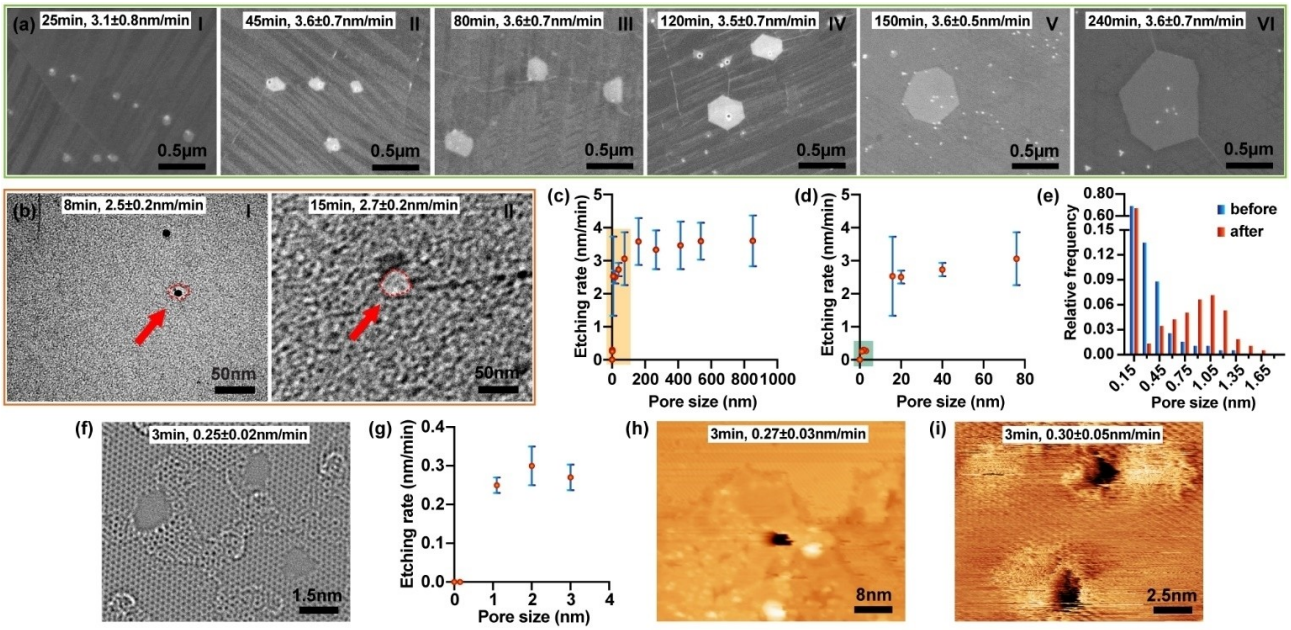

Figure 4. Effect of pore size on expansion kinetics in the presence of 500 mTorr of CO_2 at 800 °C. a) SEM images of expanded pores at progressively increasing etching times of 25, 45, 80, 120, 150, and 240 min. b) TEM images of expanded pores at 8 and 15 min. c) Evolution of the etching rate versus pore size. d) The magnified plot of the yellow-colored area in panel c. e) PSD corresponding to expanded pores in suspended SLG before and after exposure to CO_2 for 3 min. f) AC-HRTEM image of the expanded pore at 3 min. g) The magnified plot of the green-colored area in panel d. h) STM image of an expanded pore on Cu foil after exposure to CO_2 for 3 min. i) STM image of expanded pores on HOPG after exposure to CO_2 for 3 min. The error bars in all panels refer to standard deviation. For panel (c), (d), (e), and (g), they refer to etching rate based on analysis of over 80 pores.

1000 nm, Figure 4a), consistent with our previous observation of the rate of expansion under these expansion conditions (Figure 4c). For 20–80 nm sized defects, we observed a slight drop in the expansion rate, i.e., $\approx 3.1 \pm 0.8$, 2.7 ± 0.2, and 2.5 ± 0.2 nm min^{-1} for 80, 40, and 20 nm defects, respectively (Figure 4b, d). The progressively decreasing rate can be well described by much smaller rate for expansion of vacancies with steric hinderance which reduces the overall rate of expansion as per Equation (1):

$$\text{Overall rate} = \frac{\sum_{d_i}^{d_f} r_{v_i} \Delta t_i}{\sum_{d_i}^{d_f} \Delta t_i} \quad (1)$$

where r_{v_i} and Δt_i correspond to size-dependent expansion rate and time duration of expansion, respectively, for a given size interval to arrive to the next size. d_i and d_f refer to the initial and final sizes of the pore, respectively.

To probe the size-dependent etching, we turned towards expansion behavior of sub-nanometer-sized vacancies (expansion condition identical as above) by imaging their structure and size distribution by an aberration-corrected HRTEM (AC-HRTEM). Imaging was carried out under exposure conditions which do not expand the defects during the image acquisition. To improve the pore sampling for the statistical accuracy, one requires a pore density that is much higher than intrinsic vacancy defects. Therefore, we deliberately introduced sub-nanometer-sized pores (mean pore size of 0.31 ± 0.25 nm, where pore-size is defined as the diameter of the biggest circle that fits inside the pore, Figure 4e) in suspended graphene resting on a TEM grid by O_3 treatment yielding defect density of 10^{12} cm^{-2} (Figure S9).[33] We make the following observations by comparing the PSD before and after CO_2 expansion (Figure 4c–g and S10):

- Pores with size up to 0.15 nm were not affected by the CO_2 and did not expand (Figure 4e). This is consistent with the fact that CO_2 cannot fit inside these pores, therefore, the in-plane configuration needed for the dissociative chemisorption of CO_2 is not achieved. In contrast, we observed almost complete decline in the population of pores with size of 0.30 nm where CO_2 does fit (Figure 4e).
- Mean pore size shifted from 0.30 ± 0.25 nm to 1.05 ± 0.29 nm after 3 min of etching (Figure 4e, f), which corresponds to an effective etching rate of ≈ 0.25 nm/min, more than 10-fold lower than that for the larger pores.
- Another 3 minutes of etching resulted in coalescence of nearby pores resulting in a larger pore (Figure S11). Based on the average distance between the pores before the etching and the size of the coalesced pore, an etching rate of 0.25 ± 0.12 nm min^{-1} could be estimated, consistent with the above observation.
- CO_2 only expanded the existing pores without nucleating new defects (constant pore density of $\approx 10^{12}$ cm^{-2} before and after exposure to CO_2) consistent with our previous conclusion.

The above HRTEM based results were obtained on suspended graphene while our SEM observation for larger pores were based on graphene resting on Cu foil. To understand whether or not the Cu foil contributed to the observed differences, we carried out STM of CO_2-expanded pores in graphene resting on a Cu foil where pores were incorporated using the same conditions as those in the TEM study. We observed similar slow expansion rate for nanometer-sized vacancies (0.27 nm min^{-1}), which rules out any significant effect of Cu foil (Figure 4h and S12). This was further confirmed by another experiment using freshly-cleaved highly-oriented pyrolytic graphite (HOPG) where 0.8 nm pores expanded to 1.7 nm with a similar etching rate (0.30 nm min^{-1}; Figure 4i and S13). These sets of experiments validate the slower etching kinetics in nanometer-scale pores.

Next, we demonstrate an interesting use of CO_2-led expansion in identifying the location of intrinsic vacancy defects with respect to the graphene grain boundaries. Recent studies on understanding the origin of intrinsic vacancy defects in as-synthesized CVD graphene using STM, HRTEM and gas permeation studies point to two separate origins;[32,36,42] i) an incomplete intergrowth of misaligned graphene grains leading to grain-boundary defects,[28,29,43] and ii) etching of the graphene lattice in the presence of residual/leaked oxygen in the CVD reactor marked by the presence of intragrain defects.[30,31] Size and density of these defects are sensitive to the CVD environment (precursor, temperature, pressure, relative concentrations of precursors, etc.) and the catalytic substrate.[11,29,31,36,44,45] Currently, there is a lack of characterization technique which can distinguish between the relative population of grain boundary and intragrain defects. This is mainly because these defects are present in a low density and it is extremely challenging to search them in high-resolution mode in HRTEM. Given that expansion of vacancy defects makes it much easier to search and visualize them by electron microscopy, we set out to map the locations of intrinsic vacancy defects using bright-field and dark-field transmission electron microscopy (BF-TEM and DF-TEM, respectively).

DF-TEM images representing different grain orientations were false colored and superimposed on top of each other to display the orientation of graphene grains and the location of expanded vacancy defects with respect to the grain boundaries (Figures 5 and S8, also see Note S4). The vacancies appear black due to a lack of diffraction and were not false colored (Figure 5b and S8b). White and yellow arrows point out vacancies located completely inside a graphene grain and at grain boundaries, respectively. Visualization in this straightforward manner confirms that the intrinsic vacancy defects were present both at the grain boundaries as well as inside the grain away from the grain boundary (Figure 5b). The presence of intragrain vacancy defect is a strong proof for the etching of lattice in the presence of residual oxygen in the CVD reactor. Nevertheless, our finding confirms that both abovementioned origins contribute to the intrinsic vacancy defects in graphene. We note that the density of defects at the grain boundary was several folds higher than that of intragrain defects indicating that intrinsic vacancy defects do tend to primarily originate at the grain boundaries. Therefore, the studies focusing on manipulating the intrinsic defect density should primarily focus on manipulating the grain density or grain orientation to improve the stitching of the grains.

Conclusion

This study establishes CO_2 as a highly promising etchant for controlled manipulation of graphene edges and vacancy defects down to a rate of a few Å per minute. The theoretical literature predicts that CO_2 should not nucleate pores in graphene because of an extremely high energy

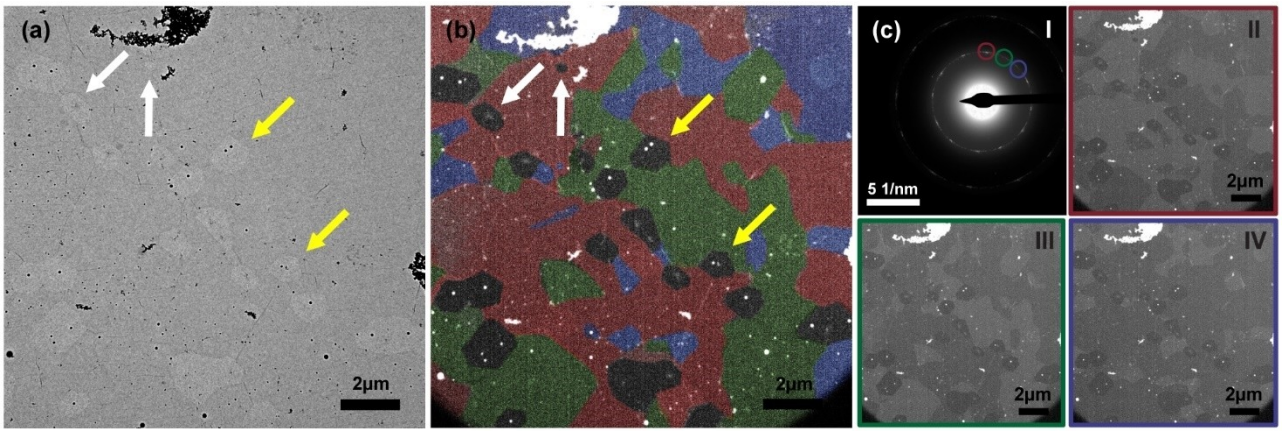

Figure 5. Visualization of the location of intrinsic vacancy defects with respect to the grain boundaries. a) BF-TEM image of suspended graphene where intrinsic defects are expanded with CO_2 at 950 °C, and corresponding false-colored DF-TEM image (b). White arrows and yellow arrows point out the pores completely inside a graphene grain and at the grain boundaries, respectively. c-I) Selected area electron diffraction pattern (SAED) and corresponding DF-TEM images from the selected diffraction spots (highlighted by red, green and purple circles) differentiated by the matching frame colors (c-II, c-III, and c-IV).

barrier for its chemisorption on the basal plane of graphene. This systematic pore expansion study, tracking the density of expanded pores as a function of etching condition, not only confirms the theoretical prediction but also reveals that only vacancy defects larger than 0.30 nm can be expanded by CO_2. So far, the energetics for CO_2-led etching of graphene edges were only studied by computational calculations and no experimental data was available. This study, for the first time, validates that CO_2 expands graphene edges with an energy barrier is 2.7 eV, close to that predicted for the dissociative chemisorption of CO_2 on the zigzag edges.

Two pieces of evidence are presented to reveal another finding. CO_2 experiences an additional energy barrier for expanding the nanometer-scale vacancies compared to the pore that are several nanometers in size. The evidence is: i) the density of expanded pores increases exponentially as a function of the etching temperature resulting from the activation of small vacancy defects at high temperature, and ii) a much-reduced rate of expansion for nanometer-scale pores compared to larger pores.

These results present a novel tool for the manipulation of vacancy defects in graphene with an added advantage of highly controlled size manipulation decoupling pore nucleation from pore expansion. This will inspire and aid future studies aiming to tune the PSD in graphene for molecular separation and sensing studies. It will also aid efforts to manipulate the width of graphene nanoribbons to control their electronic properties. Finally, CO_2 etching will also find application in the mapping of the intrinsic vacancy defect with respect to grain boundaries, a method which can be extremely useful for researchers looking to control or manipulate the intrinsic defects.

Acknowledgements

The authors acknowledge the host institution, EPFL, for the generous support. This project was funded by the Swiss National Science Foundation under the Assistance Professor Energy Grant (grant number PYAPP2_173645) and the European Research Council Starting Grant (grant number 804537). Open access funding provided by Ecole Polytechnique Federale de Lausanne.

Conflict of Interest

The authors declare no conflict of interest.

Data Availability Statement

The data that support the findings of this study are available in the supplementary material of this article.

Keywords: CO_2 Based Etching · Grain-Boundary Defects · Intrinsic Vacancy Defects · Single-Layer Graphene · Vacancy Defects · Vacancy Expansion · Vacancy Nucleation

[1] M. Z. Hossain, J. E. Johns, K. H. Bevan, H. J. Karmel, Y. T. Liang, S. Yoshimoto, K. Mukai, T. Koitaya, J. Yoshinobu, M. Kawai, A. M. Lear, L. L. Kesmodel, S. L. Tait, M. C. Hersam, *Nat. Chem.* **2012**, *4*, 305–309.
[2] J. R. Hahn, H. Kang, S. M. Lee, Y. H. Lee, *J. Phys. Chem. B* **1999**, *103*, 9944–9951.
[3] R. T. Yang, K. L. Yang, *Carbon* **1985**, *23*, 537–547.
[4] R. T. Yang, C. Wong, *Science* **1981**, *214*, 437–438.
[5] M. Yagmurcukardes, F. M. Peeters, R. T. Senger, H. Sahin, *Appl. Phys. Rev.* **2016**, *3*, 041302.
[6] M. Ezawa, *Phys. Rev. B* **2007**, *76*, 245415.
[7] J. Bai, X. Zhong, S. Jiang, Y. Huang, X. Duan, *Nat. Nanotechnol.* **2010**, *5*, 190–194.
[8] H. Sun, L. Wu, W. Wei, X. Qu, *Mater. Today* **2013**, *16*, 433–442.
[9] C. Cheng, S. A. Iyengar, R. Karnik, *Nat. Nanotechnol.* **2021**, *16*, 989–995.
[10] P. Chaturvedi, I. V. Vlassiouk, D. A. Cullen, A. J. Rondinone, N. V. Lavrik, S. N. Smirnov, *ACS Nano* **2019**, *13*, 12109–12119.
[11] P. R. Kidambi, G. D. Nguyen, S. Zhang, Q. Chen, J. Kong, J. Warner, A. Li, R. Karnik, *Adv. Mater.* **2018**, *30*, 1804977.
[12] Y. Yamada, K. Murota, R. Fujita, J. Kim, A. Watanabe, M. Nakamura, S. Sato, K. Hata, P. Ercius, J. Ciston, C. Y. Song, K. Kim, W. Regan, W. Gannett, A. Zettl, *J. Am. Chem. Soc.* **2014**, *136*, 2232–2235.
[13] J. Zhao, G. He, S. Huang, L. F. Villalobos, M. Dakhchoune, H. Bassas, K. V. Agrawal, *Sci. Adv.* **2019**, *5*, eaav1851.
[14] S. Li, M. T. Vahdat, S. Huang, K.-J. Hsu, M. Rezaei, M. Mensi, N. Marzari, K. V. Agrawal, *JACS Au* **2022**, https://doi.org/10.1021/jacsau.1c00570.
[15] D. L. Biederman, A. J. Miles, F. J. Vastola, P. L. Walker, *Carbon* **1976**, *14*, 351–356.
[16] J. F. Strange, P. L. Walker, *Carbon* **1976**, *14*, 345–350.
[17] J. Zhang, K. Jia, L. Lin, W. Zhao, H. T. Quang, L. Sun, T. Li, Z. Li, X. Liu, L. Zheng, R. Xue, J. Gao, Z. Luo, M. H. Rummeli, Q. Yuan, H. Peng, Z. Liu, *Angew. Chem. Int. Ed.* **2019**, *58*, 14446–14451; *Angew. Chem.* **2019**, *131*, 14588–14593.
[18] D. Zhao, H. Liu, C. Sun, L. Xu, Q. Cao, *Combust. Flame* **2018**, *197*, 471–486.
[19] P. Cabrera-Sanfelix, *J. Phys. Chem. A* **2009**, *113*, 493–498.
[20] A. Montoya, F. Mondragón, T. N. Truong, *Fuel Process. Technol.* **2002**, *77–78*, 125–130.
[21] M. J. Roberts, R. C. Everson, G. Domazetis, H. W. J. P. Neomagus, J. M. Jones, C. G. C. E. Van Sittert, G. N. Okolo, D. Van Niekerk, J. P. Mathews, *Carbon* **2015**, *93*, 295–314.
[22] Z. H. H. Zhu, J. Finnerty, G. Q. Q. Lu, R. T. T. Yang, *Energy Fuels* **2002**, *16*, 1359–1368.
[23] A. Montoya, F. Mondragón, T. N. Truong, *J. Phys. Chem. A* **2002**, *106*, 4236–4239.
[24] L. R. Radovic, *J. Am. Chem. Soc.* **2009**, *131*, 17166–17175.
[25] X. Yang, B. Hu, Y. Jin, W. Zhao, Z. Luo, Z. Lu, L. Fang, H. Ruan, *Adv. Mater. Interfaces* **2017**, *4*, 1601065.
[26] X. Li, W. Cai, J. An, S. Kim, J. Nah, D. Yang, R. Piner, A. Velamakanni, I. Jung, E. Tutuc, S. K. Banerjee, L. Colombo, R. S. Ruoff, *Science* **2009**, *324*, 1312–1314.
[27] A. C. Ferrari, D. M. Basko, *Nat. Nanotechnol.* **2013**, *8*, 235–246.
[28] J. Červenka, C. F. J. Flipse, *Phys. Rev. B* **2009**, *79*, 195429.
[29] L. F. Villalobos, C. Van Goethem, K. Hsu, S. Li, M. Moradi, K. Zhao, M. Dakhchoune, S. Huang, Y. Shen, E. Oveisi, V. Boureau, K. V. Agrawal, *Proc. Natl. Acad. Sci. USA* **2021**, *118*, e2022201118.
[30] P. R. Kidambi, B. C. Bayer, R. Blume, Z.-J. Wang, C. Baehtz, R. S. Weatherup, M.-G. Willinger, R. Schloegl, S. Hofmann, *Nano Lett.* **2013**, *13*, 4769–4778.
[31] Z. Yuan, G. He, S. Faucher, M. Kuehne, S. X. Li, D. Blankschtein, M. S. Strano, *Adv. Mater.* **2021**, *33*, 2104308.

[32] S. Huang, M. Dakhchoune, W. Luo, E. Oveisi, G. He, M. Rezaei, J. Zhao, D. T. L. Alexander, A. Züttel, M. S. Strano, K. V. Agrawal, *Nat. Commun.* **2018**, *9*, 2632.
[33] S. Huang, S. Li, L. F. Villalobos, M. Dakhchoune, M. Micari, D. J. Babu, M. T. Vahdat, M. Mensi, E. Oveisi, K. V. Agrawal, *Sci. Adv.* **2021**, *7*, eabf0116.
[34] L. Wang, M. S. H. Boutilier, P. R. Kidambi, D. Jang, N. G. Hadjiconstantinou, R. Karnik, *Nat. Nanotechnol.* **2017**, *12*, 509–522.
[35] N. Lisi, T. Dikonimos, F. Buonocore, M. Pittori, R. Mazzaro, R. Rizzoli, S. Marras, A. Capasso, *Sci. Rep.* **2017**, *7*, 9927.
[36] M. Rezaei, S. Li, S. Huang, K. V. Agrawal, *J. Membr. Sci.* **2020**, *612*, 118406.
[37] M. Scardamaglia, C. Struzzi, A. Zakharov, N. Reckinger, P. Zeller, M. Amati, L. Gregoratti, *ACS Appl. Mater. Interfaces* **2019**, *11*, 29448–29457.
[38] P. R. Kidambi, R. A. Terry, L. Wang, M. S. H. Boutilier, D. Jang, J. Kong, R. Karnik, *Nanoscale* **2017**, *9*, 8496–8507.
[39] L. G. Cançado, A. Jorio, E. H. M. M. Ferreira, F. Stavale, C. A. Achete, R. B. Capaz, M. V. O. O. Moutinho, A. Lombardo, T. S. Kulmala, A. C. Ferrari, *Nano Lett.* **2011**, *11*, 3190–3196.
[40] A. M. Oyarzún, X. García-Carmona, L. R. Radovic, *Carbon* **2020**, *164*, 85–99.
[41] P. Koskinen, S. Malola, H. Häkkinen, *Phys. Rev. Lett.* **2008**, *101*, 115502.
[42] K. V. Agrawal, J. D. Benck, Z. Yuan, R. P. Misra, A. Govind Rajan, Y. Eatmon, S. Kale, X. S. Chu, D. O. Li, C. Gong, J. Warner, Q. H. Wang, D. Blankschtein, M. S. Strano, *J. Phys. Chem. C* **2017**, *121*, 14312–14321.
[43] J. Coraux, A. T. N′Diaye, M. Engler, C. Busse, D. Wall, N. Buckanie, F.-J. Meyer zu Heringdorf, R. van Gastel, B. Poelsema, T. Michely, *New J. Phys.* **2009**, *11*, 023006.
[44] M. H. Khan, M. Moradi, M. Dakhchoune, M. Rezaei, S. Huang, J. Zhao, K. V. Agrawal, *Carbon* **2019**, *153*, 458–466.
[45] K. Choi, A. Droudian, R. M. Wyss, K.-P. Schlichting, H. G. Park, *Sci. Adv.* **2018**, *4*, eaau0476.

Manuscript received: January 7, 2022
Accepted manuscript online: March 4, 2022
Version of record online: March 16, 2022